ASC Report No. 17/2010

High-Order Compact Finite Difference Scheme for Option Pricing in Stochastic Volatility Models

Bertram Düring, Michel Fournié

Institute for Analysis and Scientific Computing
Vienna University of Technology — TU Wien
www.asc.tuwien.ac.at ISBN 978-3-902627-03-2

Most recent ASC Reports

16/2010 *Robert Hammerling, Othmar Koch, Christa Simon, Ewa B. Weinmüller*
Numerical Treatment od Singular ODE EVPs Using `bvpsuite`

15/2010 *Ansgar Jüngel, René Pinnau, Elisa Röhrig*
Analysis of a Bipolar Energy-Transport Model for a Metal-Oxide-Semiconductor Diode

14/2010 *Markus Aurada, Michael Ebner, Michael Feischl, Samuel Ferraz-Leite, Petra Goldenits, Michael Karkulik, Markus Mayr, Dirk Praetorius*
Hilbert (Release 2): A MATLAB Implementation of Adaptive BEM

13/2010 *Alexander Dick, Othmar Koch, Roswitha März, Ewa Weinmüller*
Convergence of Collocation Schemes for Nonlinear Index 1 DAEs with a Singular Point

12/2010 *Markus Aurada, Samuel Ferraz-Leite, Petra Goldenits, Michael Karkulik, Markus Mayr, Dirk Praetorius*
Convergence of Adaptive BEM for some Mixed Boundary Value Problem

11/2010 *Mario Bukal, Ansgar Jüngel, Daniel Matthes*
Entropies for Radially Symmetric Higher-Order Nonlinear Diffusion Equations

10/1010 *Karl Rupp, Ansgar Jüngel, Karl-Tibor Grasser*
Matrix Compression for Spherical Harmonics Expansions of the Boltzmann Transport Equation for Semiconductors

9/2010 *Markus Aurada, Samuel Ferraz-Leite, Dirk Praetorius*
Estimator Reduction and Convergence of Adaptive BEM

8/2010 *Robert Hammerling, Othmar Koch, Christa Simon, Ewa B. Weinmüller*
Numerical Solution of singular Eigenvalue Problems for ODEs with a Focus on Problems Posed on Semi-Infinite Intervals

7/2010 *Robert Hammerling, Othmar Koch, Christa Simon, Ewa B. Weinmüller*
Numerical Solution of Singular ODE Eigenvalue Problems in Electronic Structure Computations

Institute for Analysis and Scientific Computing
Vienna University of Technology
Wiedner Hauptstraße 8–10
1040 Wien, Austria

E-Mail: `admin@asc.tuwien.ac.at`
WWW: `http://www.asc.tuwien.ac.at`
FAX: `+43-1-58801-10196`

ISBN 978-3-902627-03-2

ASC
TU WIEN

High-order compact finite difference scheme for option pricing in stochastic volatility models

Bertram Düring[a,*], Michel Fournié[b]

[a]*Institut für Analysis und Scientific Computing, Technische Universität Wien, Wiedner Hauptstraße 8–10, 1040 Wien, Austria.*
[b]*Institut de Mathématiques de Toulouse, Equipe 'Mathématiques pour l'Industrie et la Physique', CNRS, Unité Mixte 5219, Université Paul Sabatier, 118, route de Narbonne, 31062 Toulouse Cedex, France.*

Abstract

We derive a new compact high-order finite difference scheme for option pricing in stochastic volatility models. The scheme is fourth order accurate in space and second order accurate in time. To prove results on the unconditional stability in the sense of von Neumann we perform a thorough Fourier analysis of the problem and deduce convergence of our scheme. We present results of numerical experiments for the European and American option pricing problem.

Keywords: Option pricing, compact finite difference discretizations, mixed derivatives, free boundary problem
2000 MSC: 65M06, 65M12, 91B28

1. Introduction

The traditional approach to price derivative assets or options is to specify an asset price process exogenously by a stochastic diffusion process and then price by no-arbitrage arguments. The seminal example of this approach is Black & Scholes' paper [2] on pricing of European-style options. This approach leads to simple, explicit pricing formulas. However, empirical re-

*Corresponding author
Email addresses: bduering@anum.tuwien.ac.at (Bertram Düring), michel.fournie@math.univ-toulouse.fr (Michel Fournié)

search has revealed that they are not able to explain important effects in real financial markets, e.g. the volatility smile (or skew) in option prices.

In real financial markets, not only asset returns are subject to risk, but also the estimate of the riskiness is typically subject to significant uncertainty. To incorporate such additional source of randomness into an asset pricing model, one has to introduce a second risk factor. This also allows to fit higher moments of the asset return distribution. The most prominent work in this direction is Heston's model [7]. Such models are based on a two-dimensional stochastic diffusion process with two Brownian motions with correlation ρ, i.e., $dW^{(1)}(t)dW^{(2)}(t) = \rho\, dt$, on a given filtered probability space for the stock price $S = S(t)$ and the stochastic volatility $\sigma = \sigma(t)$,

$$\begin{aligned} dS(t) &= \bar{\mu} S(t)\, dt + \sqrt{\sigma(t)} S(t)\, dW^{(1)}(t), \\ d\sigma(t) &= a(\sigma(t))\, dt + b(\sigma(t))\, dW^{(2)}(t), \end{aligned}$$

where $\bar{\mu}$ is the drift of the stock, $a(\sigma)$ and $b(\sigma)$ are the drift and the diffusion coefficient of the stochastic volatility.

Application of Itô's lmma leads to partial differential equations of the following form

$$V_t + \frac{1}{2} S^2 \sigma V_{SS} + \rho b(\sigma) \sqrt{\sigma} S V_{S\sigma} + \frac{1}{2} b^2(\sigma) V_{\sigma\sigma} + a(\sigma) V_\sigma + rSV_S - rV = 0, \quad (1)$$

where r is the (constant) riskless interest rate. Equation (1) has to be solved for $S, \sigma > 0$, $0 \le t \le T$ and subject to final and boundary conditions which depend on the specific option that is to be priced.

For some models and under additional restrictions, closed form solutions to (1) can be obtained by Fourier methods (e.g. [7], [6]). Another approach is to derive approximate analytic expressions, see e.g. [1] and the literature cited therein. In general, however, —even in the Heston model [7] when the coefficients in it are non constant— equation (1) has to be solved numerically. Moreover, many (so-called American) options feature an additional early exercise right. Then one has to solve a free boundary problem which consists of (1) and an early exercise constraint for the option price. Also for this problem one typically has to resort to numerical approximations.

In the mathematical literature, there are many papers on numerical methods for option pricing, mostly addressing the case of a single risk factor and using standard, second order finite difference methods (see, e.g., [17] and the references therein). More recently, higher-order finite difference schemes

(fourth-order in space) were proposed that use a compact stencil (three points in space). In the present context see, e.g., [16] for linear and [4, 5, 11] for fully nonlinear problems.

There are less works considering numerical methods for option pricing in stochastic volatility models, i.e., for two spatial dimensions. Finite difference approaches that are used are often standard, low order methods (second order in space) and do provide little numerical analysis or convergence results. Other approaches include finite element-finite volume [19], multigrid [3], sparse wavelet [10], and spectral methods [18].

Let us review some of the related finite difference literature. Different efficient methods for solving the American option pricing problem for the Heston model are compared in [9]. The article focusses on the treatment of the early exercise free boundary and uses a second order finite difference discretization. In [8] different, low order ADI (alternating direction implicit) schemes are adapted to the Heston model to include the mixed spatial derivative term. While most of [16] focusses on a compact high-order scheme for the standard (one-dimensional) case, in a short remark [16, Section 5] also the stochastic volatility (two-dimensional) case is considered. However, the final scheme there is of second order only due to the low order approximation of the cross diffusion term.

The originality of the present work consists in proposing a new, *compact finite difference scheme* for (two-dimensional) option pricing models with *stochastic volatility*. It should be emphasized that although our presentation is focused on the Heston model, our methodology easily adapts to a other stochastic volatility models. We derive a new compact scheme that is fourth order accurate in space and second order accurate in time. To prove results on the unconditional stability in the sense of von Neumann we perform a thorough Fourier analysis of the problem and deduce convergence of our scheme.

This paper is organized as follows. In the next section, we recall the Heston model from [7] and its closed form solution for the constant coefficient case. In Section 3 we introduce new independent variables to transform the partial differential equation to a more tractable form. In Section 4 we derive the new high-order compact scheme. We analyse its stability and deduce a convergence result. Numerical experiments that confirm the good properties of the method are presented in Section 5. We give numerical results for the European and the American option pricing problem.

2. Heston model

Let us recall the Heston model from [7] on which we will focus our presentation. Note that our method carries over naturally to other stochastic volatility models with different choices of the drift and the diffusion coefficient of the stochastic volatility. Consider a two-dimensional standard Brownian motion $W = (W^{(1)}, W^{(2)})$ with correlation $dW^{(1)}(t)dW^{(2)}(t) = \rho dt$ on a given filtered probability space. Assuming a specific form of the drift $a(\sigma)$ and the diffusion coefficient $b(\sigma)$ of the stochastic volatility, the value of the underlying asset in [7] is characterized by

$$\begin{aligned} dS(t) &= \bar{\mu} S(t)\, dt + \sqrt{\sigma(t)} S(t)\, dW^{(1)}(t), \\ d\sigma(t) &= \kappa^*(\theta^* - \sigma(t))\, dt + v\sqrt{\sigma(t)}\, dW^{(2)}(t), \end{aligned} \tag{2}$$

for $0 < t \leq T$ with $S(0), \sigma(0) > 0$ and $\bar{\mu}$, κ^*, v and θ^* the drift, the mean reversion speed, the volatility of volatility and the long-run mean of σ, respectively.

By Itô's lemma and standard arbitrage arguments it follows that any derivative asset $V = V(S, \sigma, t)$ solves the following partial differential equation

$$\begin{aligned} V_t + \frac{1}{2} S^2 \sigma V_{SS} + \rho v \sigma S V_{S\sigma} + \frac{1}{2} v^2 \sigma V_{\sigma\sigma} + r S V_S \\ + \big[\kappa^*(\theta^* - \sigma) - \lambda(S, \sigma, t)\big] V_\sigma - rV = 0, \end{aligned} \tag{3}$$

which has to be solved for $S, \sigma > 0$, $0 \leq t < T$ and subject to a suitable final condition, e.g.,

$$V(S, \sigma, T) = \max(K - S, 0)$$

in case of a European put option (with K denoting the strike price). In (3), $\lambda(S, \sigma, t)$ denotes the market price of volatility risk. While in principle it could be estimated from market data, this is difficult in practice and the results are controversial. Therefore, one typically assumes a risk premium that is proportional to σ and chooses $\lambda(S, \sigma, t) = \lambda_0 \sigma$ for some constant λ_0. For streamlining the presentation we restrict ourselves to this important case, although our scheme applies to general functional forms $\lambda = \lambda(S, \sigma, t)$.

The 'boundary' conditions in the case of the put option read as follows

$$V(0, \sigma, t) = K e^{-r(T-t)}, \qquad T > t \geq 0,\ \sigma > 0, \tag{4a}$$

$$V(S, \sigma, t) \to 0, \qquad T > t \geq 0,\ \sigma > 0,\ \text{as } S \to \infty, \tag{4b}$$

$$V_\sigma(S, \sigma, t) \to 0, \qquad T > t \geq 0,\ S > 0,\ \text{as } \sigma \to \infty. \tag{4c}$$

The remaining boundary condition at $\sigma = 0$ can be obtained by looking at the formal limit $\sigma \to 0$ in (3), i.e.,

$$V_t + rSV_S + \kappa^*\theta^* V_\sigma - rV = 0, \quad T > t \geq 0,\ S > 0,\ \text{as } \sigma \to 0. \tag{4d}$$

This boundary condition is used frequently, e.g. in [9, 19], but does not seem very practicable. Alternatively, one can use a homogeneous Neumann condition [3], i.e.,

$$V_\sigma(S, \sigma, t) \to 0, \quad T > t \geq 0,\ S > 0,\ \text{as } \sigma \to 0. \tag{4e}$$

For *constant* parameters, one can employ Fourier transform techniques and obtain a system of ordinary differential equations which can be solved analytically [7]. By inverting the transform one arrives at a closed-form solution of (3), where the European put option price V is given by

$$V(S, \sigma, t) = Ke^{-r(T-t)}\mathcal{I}_2 - S\mathcal{I}_1, \tag{5}$$

with $(k = 1, 2)$

$$\mathcal{I}_k = \frac{1}{2} + \frac{1}{\pi}\int_0^\infty \mathrm{Re}\left[\frac{e^{-i\xi \ln(K)} f_k(\xi)}{i\xi}\right] d\xi, \tag{6}$$

$$f_k(\xi) = \exp\big(C(T-t,\xi) + \sigma D(T-t,\xi) + i\xi \ln S\big),$$

$$C(\tau,\xi) = r\xi i\tau + \frac{\kappa^*\theta^*}{v^2}\Big[(b+d)\tau - 2\ln\Big(\frac{1-ge^{d\tau}}{1-g}\Big)\Big],\ D(\tau,\xi) = \frac{b_k + d_k}{v^2}\frac{1-e^{d_k\tau}}{1-ge^{d_k\tau}},$$

$$g = \frac{b_k + d_k}{b_k - d_k}, \quad d_k = \sqrt{(\xi^2 \mp i\xi)\, v^2 + b_k^2}, \quad b_k = \kappa^* + \lambda_0 - \rho v(i\xi + \delta_{1k}).$$

Here, $\delta_{i,j}$ denotes Kronecker's delta.

3. Transformation of the equation and boundary conditions

Under the transformation of variables

$$x = \ln\Big(\frac{S}{K}\Big), \quad \tilde{t} = T - t, \quad u = \exp(r\tilde{t})\frac{V}{K}, \tag{7}$$

(we immediately drop the tilde in the following) we arrive at

$$u_t - \frac{1}{2}\sigma\big(u_{xx} + 2\rho v u_{x\sigma} + v^2 u_{\sigma\sigma}\big) + \Big(\frac{1}{2}\sigma - r\Big)u_x - \big[\kappa^*\theta^* - (\kappa^* + \lambda_0)\sigma\big]u_\sigma = 0, \tag{8}$$

which is now posed on $\mathbb{R} \times \mathbb{R}^+$. We study the problem using the modified parameters

$$\kappa = \kappa^* + \lambda_0, \quad \theta = \frac{\kappa^* \theta^*}{\kappa^* + \lambda_0},$$

which is both convenient and standard practice. For similar reasons, some authors set the market price of volatility risk to zero. Equation (8) can then be written as

$$u_t - \frac{1}{2}\sigma\big(u_{xx} + 2\rho v u_{x\sigma} + v^2 u_{\sigma\sigma}\big) + \Big(\frac{1}{2}\sigma - r\Big)u_x - \kappa\big[\theta - \sigma\big]u_\sigma = 0. \qquad (9)$$

The problem is completed by the following initial and boundary conditions:

$$\begin{aligned}
u(x,\sigma,0) &= \max(1-\exp(x),0), && x \in \mathbb{R},\ \sigma > 0,\\
u(x,\sigma,t) &\to 1, && x \to -\infty,\ \sigma > 0,\ t > 0,\\
u(x,\sigma,t) &\to 0, && x \to +\infty,\ \sigma > 0,\ t > 0,\\
u_\sigma(x,\sigma,t) &\to 0, && x \in \mathbb{R},\ \sigma \to \infty,\ t > 0,\\
u_\sigma(x,\sigma,t) &\to 0, && x \in \mathbb{R},\ \sigma \to 0,\ t > 0.
\end{aligned}$$

4. High order compact scheme

For the discretization, we replace $\mathbb{R}$ by $[-R_1, R_1]$ and $\mathbb{R}^+$ by $[0, R_2]$ with $R_1, R_2 > 0$. For simplicity, we consider a uniform grid $Z = \{x_i \in [-R_1, R_1] : x_i = ih_1,\ i = -N, ..., N\} \times \{\sigma_j \in [0, R_2] : \sigma_j = jh_2,\ i = 0, ..., M\}$ consisting of $(2N+1)\times(M+1)$ grid points, with $R_1 = Nh_1$, $R_2 = Mh_2$ and with space steps h_1, h_2 and time step k. Let $u^n_{i,j}$ denote the approximate solution of (9) in (x_i, σ_j) at the time $t_n = nk$ and let $u^n = (u^n_{i,j})$.

The boundary conditions on the grid are treated as follows. Dirichlet conditions are used on two boundaries

$$u^n_{-N,j} = 1, \quad u^n_{+N,j} = 0, \quad (j = 0, \ldots, M),$$

while homogeneous Neumann conditions are used at the other boundaries. We impose artificial boundary conditions in a classical manner rigorously studied for a class of Black-Scholes equations in [12].

4.1. Derivation of the high-order scheme for the elliptic problem

First we introduce the high-order compact finite difference discretization for the stationary, elliptic problem with Laplacian operator which appears

after the variable transformation $y = \sigma/v$. Equation (9) is then reduced to the two-dimensional elliptic equation

$$-\frac{1}{2}vy(u_{xx}+u_{yy})-\rho vyu_{xy}+\Big(\frac{1}{2}vy-r\Big)u_x-\kappa\frac{\theta-vy}{v}u_y=f(x,y), \quad (10)$$

with the same boundary conditions.

The fourth-order compact finite difference scheme uses a nine-point computational stencil using the eight nearest neighboring points of the reference grid point (i, j).

The idea behind the derivation of the high-order compact scheme is to operate on the differential equations as an auxiliary relation to obtain finite difference approximations for high-order derivatives in the truncation error. Inclusion of these expressions in a central difference method for equation (10) increases the order of accuracy, typically to $\mathcal{O}(h^4)$, while retaining a compact stencil defined by nodes surrounding a grid point.

Introducing a uniform grid with mesh spacing h in both the x- and y-direction, the standard central difference approximation to equation (10) at grid point (i, j) is

$$\begin{aligned}-\frac{1}{2}vy_j\big(\delta_x^2u_{i,j}+\delta_y^2u_{i,j}\big)-\rho vy_j\delta_x\delta_yu_{i,j}\\ +\Big(\frac{1}{2}vy_j-r\Big)\delta_xu_{i,j}-\kappa\frac{\theta-vy_j}{v}\delta_yu_{i,j}-\tau_{i,j}=f_{i,j},\end{aligned} \quad (11)$$

where δ_x and δ_x^2 (δ_y and δ_y^2, respectively) denote the first and second order central difference approximations with respect to x (with respect to y). The associated truncation error is given by

$$\begin{aligned}\tau_{i,j}=\frac{1}{24}vyh^2(u_{xxxx}+u_{yyyy})+\frac{1}{6}\rho vyh^2(u_{xyyy}+u_{xxxy})\\ +\frac{1}{12}(2\,r-vy)h^2u_{xxx}+\frac{1}{6}\frac{\kappa(\theta-vy)}{v}h^2u_{yyy}+\mathcal{O}(h^4).\end{aligned} \quad (12)$$

For the sake of readability, here and in the following we omit the subindices j and (i, j) on y_j and $u_{i,j}$ (and its derivatives), respectively. We now seek second-order approximations to the derivatives appearing in (12). Differen-

tiating equation (10) once with respect to x and y, respectively, yields

$$u_{xxx} = -u_{xyy} - 2\rho u_{xxy} - \frac{2r+vy}{vy}u_{xx} + 2\frac{\kappa(vy-\theta)}{v^2y}u_{xy} - \frac{2}{vy}f_x, \tag{13}$$

$$u_{yyy} = -u_{xxy} - 2\rho u_{xyy} - \frac{1}{y}u_{xx} - \frac{2\kappa(\theta-vy)+v^2}{v^2y}u_{yy} - \frac{2\rho+2r-vy}{vy}u_{xy} + \frac{1}{y}u_x + \frac{2\kappa}{vy}u_y - \frac{2}{vy}f_y. \tag{14}$$

Differentiating equations (13) and (14) with respect to y and x, respectively, and adding the two expressions, we obtain

$$u_{xyyy} + u_{xxxy} = \frac{vy+2r}{2vy^2}u_{xx} + \frac{\kappa(\theta+vy)}{v^2y^2}u_{xy} - \frac{4\kappa(\theta-vy)+v^2}{2v^2y}u_{xyy} - \frac{\rho v+2r-vy}{vy}u_{xxy} - 2\rho u_{xxyy} - \frac{1}{2y}u_{xxx} + \frac{1}{vy^2}f_x - \frac{2}{vy}f_{xy}. \tag{15}$$

Notice that all the terms in the right hand sides of (13)-(15) have compact $\mathcal{O}(h^2)$ approximations at node (i,j) using finite difference based on δ_x, δ_x^2, δ_y, δ_y^2. We have for example $u_{xxy_{i,j}} = \delta_x^2\delta_y u_{i,j} + \mathcal{O}(h^2)$. By differentiating equation (10) twice with respect to x and y, respectively, and adding the two expressions, we obtain

$$u_{xxxx} + u_{yyyy} = -2\rho u_{xyyy} - 2\rho u_{xxxy} - 2u_{xxyy} + 2\frac{(\kappa vy - v^2 - \kappa\theta)}{v^2y}u_{xxy} - \frac{(2r-vy)}{vy}u_{xxx} + 2\frac{(\kappa vy - v^2 - \kappa\theta)}{v^2y}u_{yyy} - \frac{(-vy+4\rho v+2r)}{vy}u_{xyy} + 4\frac{\kappa}{vy}u_{yy} + \frac{2}{y}u_{xy} - \frac{2}{vy}(f_{xx}+f_{yy}). \tag{16}$$

Again, using (13)-(15), the right hand side can be approximated up to $\mathcal{O}(h^2)$ within the nine-point compact stencil. Substituting equations (13)-(16) into equation (12) and simplifying yields a new expression for the error term $\tau_{i,j}$ that consists only of terms which are either

- terms of order $\mathcal{O}(h^4)$, or
- terms of order $\mathcal{O}(h^2)$ multiplied by derivatives of u which can be approximated up to $\mathcal{O}(h^2)$ within the nine-point compact stencil.

Hence, substituting the central $\mathcal{O}(h^2)$ approximations to the derivatives in this new expression for the error term and inserting it into (11) yields the following $\mathcal{O}(h^4)$ approximation to the initial partial differential equation (10),

$$
\begin{aligned}
&-\frac{1}{24}\frac{h^2((vy_j-2r)^2-4\rho vr-2\kappa(vy_j-\theta)-2v^2)+12v^2y_j^2}{vy_j}\delta_x^2u_{i,j}\\
&-\frac{1}{12}\frac{h^2(2\kappa^2(vy_j-\theta)^2-\kappa v^3y_j-\kappa\theta v^2-v^4)+6v^4y_j^2}{v^3y_j}\delta_y^2u_{i,j}\\
&-\frac{1}{12}h^2vy_j(1+2\rho^2)\delta_x^2\delta_y^2u_{i,j}\\
&+\frac{h^2}{6}\frac{(\kappa(vy_j-\theta)+v\rho(vy_j-2r))}{v}\delta_x^2\delta_yu_{i,j}\\
&+\frac{h^2}{12}\frac{(4\kappa\rho(vy_j-\theta)+v(vy_j-2r))}{v}\delta_x\delta_y^2u_{i,j}\\
&-\frac{1}{6}\frac{h^2(\kappa(vy_j-2r)(vy_j-\theta)-\kappa v^2y_j\rho-v^3\rho-v^2r)+6v^3y_j^2\rho}{v^2y_j}\delta_x\delta_yu_{i,j}\\
&+\frac{1}{12}\frac{6v^2y_j^2-12vy_jr-h^2[v^2+\kappa(vy_j-\theta)]}{vy_j}\delta_xu_{i,j}\\
&+\frac{\kappa}{6}\frac{(6v^2y_j^2-6vy_j\theta-h^2[v^2+\kappa(vy_j-\theta)])}{v^2y_j}\delta_yu_{i,j}\\
=&f_{i,j}+\frac{h^2}{6}\frac{\rho}{v}\delta_x\delta_yf_{i,j}-\frac{h^2}{6}\frac{(v^2+\kappa(vy_j-\theta))}{v^2y_j}\delta_yf_{i,j}\\
&-\frac{h^2}{12}\frac{(2\rho v-2r+vy_j)}{vy_j}\delta_xf_{i,j}+\frac{h^2}{12}\delta_x^2f_{i,j}+\frac{h^2}{12}\delta_y^2f_{i,j}.
\end{aligned}
\tag{17}
$$

The fourth-order compact finite difference scheme (17) considered at the mesh point (i,j) involves the nearest eight neighboring mesh points. Associated to the shape of the computational stencil, we introduce indexes for each node from 0 to 9,

$$
\begin{pmatrix}
u_{i-1,j+1}=u_6 & u_{i,j+1}=u_2 & u_{i+1,j+1}=u_5\\
u_{i-1,j}=u_3 & u_{i,j}=u_0 & u_{i+1,j}=u_1\\
u_{i-1,j-1}=u_7 & u_{i,j-1}=u_4 & u_{i+1,j-1}=u_8
\end{pmatrix}.
\tag{18}
$$

With this indexing, the scheme (17) is defined by

$$
\sum_{l=0}^{8}\alpha_lu_l=\sum_{l=0}^{8}\gamma_lf_l,
\tag{19}
$$

where the coefficients α_l and γ_l are given by

$$\begin{aligned}
\alpha_0 =& \left(\frac{4\kappa^2+v^2}{12v} - \frac{v(2\rho^2-5)}{3h^2}\right) y_j \\
& - \frac{\kappa v^2 + 2\kappa^2\theta + v^2 r}{3v^2} + \frac{-v^4 + \kappa^2\theta^2 - v^3 r\rho + v^2 r^2}{3v^3 y_j}, \\
\alpha_{1,3} =& \left(-\frac{v}{24} + \frac{\pm\frac{1}{6}v \mp \frac{1}{3}\kappa\rho}{h} + \frac{v(\rho^2-1)}{3h^2}\right) y_j \mp \frac{\kappa h}{24} + \frac{\kappa}{12} + \frac{r}{6} \\
& \mp \frac{vr - \kappa\theta\rho}{3vh} \mp \frac{(v^2-\kappa\theta)h}{24vy_j} - \frac{-2rv\rho + \kappa\theta + 2r^2 - v^2}{12vy_j}, \\
\alpha_{2,4} =& \left(-\frac{\kappa^2}{6v} + \frac{\pm\frac{1}{3}\kappa \mp \frac{1}{6}\rho v}{h} + \frac{v(\rho^2-1)}{3h^2}\right) y_j \mp \frac{\kappa^2 h}{12v} + \frac{\kappa(v^2+4\kappa\theta)}{12v^2} \\
& \mp \frac{rv\rho - \kappa\theta}{3vh} \mp \frac{\kappa(v^2-\kappa\theta)h}{12v^2 y_j} + \frac{(2\kappa\theta+v^2)(v^2-\kappa\theta)}{12v^3 y_j}, \\
\alpha_{5,7} =& \left(-\frac{\kappa}{24} \pm \frac{(2\rho+1)(2\kappa+v)}{24h} - \frac{v(\rho+1)(2\rho+1)}{12h^2}\right) y_j \\
& + \frac{\kappa(\rho v + 2r + \theta)}{24v} \mp \frac{(2\rho+1)(\kappa\theta+vr)}{12vh} + \frac{v^2 r + v^3\rho - 2r\kappa\theta}{24v^2 y_j}, \\
\alpha_{6,8} =& \left(\frac{\kappa}{24} \pm \frac{(2\rho-1)(-2\kappa+v)}{24h} - \frac{v(2\rho-1)(\rho-1)}{12h^2}\right) y_j \\
& - \frac{\kappa(\rho v + 2r + \theta)}{24v} \mp \frac{(2\rho-1)(vr-\kappa\theta)}{12vh} - \frac{v^2 r + v^3\rho - 2r\kappa\theta}{24v^2 y_j},
\end{aligned}$$

and

$$\begin{aligned}
&\gamma_0 = \frac{2}{3}, \qquad \gamma_5 = \gamma_7 = \frac{\rho}{24}, \qquad \gamma_6 = \gamma_8 = -\frac{\rho}{24}, \\
&\gamma_{1,3} = \frac{1}{12} \mp \frac{h}{24} \pm \frac{1}{12}\frac{(r-\rho v)h}{vy_j}, \qquad \gamma_{2,4} = \frac{1}{12} \mp \frac{1}{12}\frac{\kappa h}{v} \mp \frac{1}{12}\frac{(v^2-\kappa\theta)h}{v^2 y_j}.
\end{aligned}$$

When multiple indexes are used with $\pm$ and $\mp$ signs, the first index corresponds to the upper sign.

4.2. High-order scheme for the parabolic problem

The high-order compact approach presented in the previous section can be extended to the parabolic problem directly by considering the time derivative in place of $f(x, y)$. Any time integrator can be implemented to solve the

problem as presented in [14]. We consider the most common class of methods involving two times steps. For example, differencing at $t_\mu = (1-\mu)t^n + \mu t^{n+1}$, where $0 \le \mu \le 1$ and the superscript n denotes the time level, yields a class of integrators that include the forward Euler ($\mu = 0$), Crank-Nicolson ($\mu = 1/2$) and backward Euler ($\mu = 1$) schemes. We use the notation $\delta_t^+ u^n = \frac{u^{n+1}-u^n}{k}$. Then the resulting fully discrete difference scheme for node (i, j) at the time level n becomes

$$\sum_{l=0}^{8} \mu\alpha_l u_l^{n+1} + (1-\mu)\alpha_l u_l^n = \sum_{l=0}^{8} \gamma_l \delta_t^+ f_l^n,$$

that can be written in the form (after multiplying by $24v^3h^2yk$)

$$\sum_{l=0}^{8} \beta_l u_l^{n+1} = \sum_{l=0}^{8} \zeta_l u_l^n. \tag{20}$$

The coefficients β_l, ζ_l are numbered according to the indexes (18) and are given by

$$\begin{aligned}
\beta_0 =&(((2{y_j}^2 - 8)v^4 + ((-8\kappa - 8r)y_j - 8\rho r)v^3 + (8\kappa^2{y_j}^2 + 8r^2)v^2 \\
&- 16\kappa^2\theta v y_j + 8\kappa^2\theta^2)\mu k + 16v^3 y_j)h^2 + (-16\rho^2 + 40){y_j}^2 v^4 \mu k \\
\beta_{1,3} =&\pm((\kappa\theta v^2 - v^4 - \kappa y_j v^3)\mu k - (y_j + 2\rho)v^3 + 2v^2 r)h^3 + (((-{y_j}^2 + 2)v^4 \\
&+ ((4r + 2\kappa)y_j + 4\rho r)v^3 - (2\kappa\theta + 4r^2)v^2)\mu k + 2v^3 y_j)h^2 \\
&\pm(4v^4{y_j}^2 + (-8{y_j}^2\kappa\rho - 8y_j r)v^3 + 8y_j\kappa\theta\rho v^2)\mu k h + (8\rho^2 - 8){y_j}^2 v^4 \mu k, \\
\beta_{2,4} =&\pm((2\kappa^2\theta v - 2\kappa^2 v^2 y_j - 2v^3\kappa)\mu k - 2v^2 y_j\kappa + 2v\kappa\theta - 2v^3)h^3 + ((2v^4 \\
&+ 2\kappa y_j v^3 + (-4\kappa^2{y_j}^2 + 2\kappa\theta)v^2 + 8\kappa^2\theta v y_j - 4\kappa^2\theta^2)\mu k + 2v^3 y_j)h^2 \\
&\pm((8{y_j}^2\kappa + 8y_j\rho r)v^3 - 4v^4{y_j}^2\rho - 8v^2 y_j\kappa\theta)\mu k h + (8\rho^2 - 8){y_j}^2 v^4 \mu k, \\
\beta_{5,7} =&((v^4\rho + (-y^2\kappa + \kappa y_j\rho + r)v^3 + (\theta + 2r)\kappa y_j v^2 - 2r\kappa\theta v)\mu k \\
&+ v^3\rho y_j)h^2 \pm((2\rho + 1){y_j}^2 v^4 + ((2 + 4\rho)\kappa{y_j}^2 + (-4\rho r - 2r)y_j)v^3 \\
&+ (-2\theta - 4\theta\rho)\kappa y_j v^2)\mu k h + (-2 - 4\rho^2 - 6\rho){y_j}^2 v^4 \mu k, \\
\beta_{6,8} =&((-v^4\rho + ({y_j}^2\kappa - \kappa y_j\rho - r)v^3 + (-\theta - 2r)\kappa y_j v^2 + 2r\kappa\theta v)\mu k \\
&- v^3\rho y_j)h^2 \pm((2\rho - 1){y_j}^2 v^4 + ((2 - 4\rho)\kappa{y_j}^2 + (2r - 4\rho r)y_j)v^3 \\
&+ (4\theta\rho - 2\theta)\kappa y_j v^2)\mu k h + (-4\rho^2 + 6\rho - 2){y_j}^2 v^4 \mu k,
\end{aligned}$$

and

$$
\begin{aligned}
\zeta_0 =& 16v^3 y_j h^2 + (1-\mu)k(((8-2{y_j}^2)v^4 + ((8\kappa+8r)y_j + 8\rho r)v^3 \\
&+ (-8r^2 - 8\kappa^2 {y_j}^2)v^2 + 16\kappa^2\theta v y_j - 8\kappa^2\theta^2)h^2 + (-40+16\rho^2){y_j}^2 v^4), \\
\zeta_{1,3} =& \pm(2r - (y_j+2\rho)v)v^2h^3 + 2v^3 y_j h^2 + (1-\mu)k(\pm(v\kappa y_j + v^2 - \kappa\theta)v^2h^3 \\
&+ (v^2{y_j}^2 - (4r+2\kappa)v y_j + 4r^2 + 2\kappa\theta - 2v^2 - 4\rho v r)v^2h^2 \\
&\pm((-4v+8\kappa\rho)v^3{y_j}^2 + (-8\kappa\theta\rho + 8vr)v^2 y_j)h + (8v^2 - 8v^2\rho^2)v^2{y_j}^2), \\
\zeta_{2,4} =& \pm(2v\kappa\theta - 2v^2 y_j\kappa - 2v^3)h^3 + 2v^3 y_j h^2 + (1-\mu)k(\pm 2(v^3\kappa - \kappa^2\theta v \\
&+ \kappa^2 v^2 y_j)h^3 + (4\kappa^2 v^2 {y_j}^2 - (2v^2 + 8\kappa\theta)\kappa v y_j + 2\kappa\theta(2\kappa\theta - v^2) - 2v^4)h^2 \\
&\pm((-8v^3\kappa + 4v^4\rho){y_j}^2 + (8\kappa\theta v^2 - 8v^3\rho r)y_j)h + (-8v^4\rho^2 + 8v^4){y_j}^2), \\
\zeta_{5,7} =& v^3\rho y_j h^2 + (1-\mu)k((v^3{y_j}^2\kappa - v(v\kappa\theta + 2r\kappa v + \kappa v^2\rho)y_j \\
&- v(v^2 r - 2r\kappa\theta + v^3\rho))h^2 \pm(-v(2v^3\rho + v^3 + 4\kappa v^2\rho + 2v^2\kappa){y_j}^2 \\
&+ v(2v\kappa\theta + 4v\kappa\theta\rho + 4v^2\rho r + 2v^2 r)y_j)h + v(2v^3 + 6v^3\rho + 4v^3\rho^2){y_j}^2), \\
\zeta_{6,8} =& -v^3\rho y_j h^2 + (1-\mu)k((-v^3{y_j}^2\kappa + v(v\kappa\theta + 2r\kappa v + \kappa v^2\rho)y_j \\
&+ v(v^2 r - 2r\kappa\theta + v^3\rho))h^2 \pm(v(-2v^3\rho + v^3 + 4\kappa v^2\rho - 2v^2\kappa){y_j}^2 \\
&+ v(2v\kappa\theta - 4v\kappa\theta\rho + 4v^2\rho r - 2v^2 r)y_j)h + v(2v^3 - 6v^3\rho + 4v^3\rho^2){y_j}^2).
\end{aligned}
$$

When multiple indexes are used with $\pm$ and $\mp$ signs, the first index corresponds to the upper sign. Choosing $\mu = 1/2$, i.e., in the Crank-Nicolson case, the resulting scheme is of order two in time and of order four in space.

4.3. Convergence analysis

In this section, we study the convergence of the new scheme. Due to the linear property of the problem, we consider the consistency and the stability of the scheme.

Theorem 1. *For any fixed parameters, the scheme (20) is consistent with the partial differential equation (10).*

Proof. Trivial by construction – see sections 4.1 and 4.2. ■

We now analyse the linear von Neumann stability of the scheme (20). To reduce the high number of parameters in the following numerical analysis, we assume here zero interest rate and correlation, $r = \rho = 0$, and choose the parameter $\mu = 1/2$ (Crank-Nicolson case). In our numerical experiments we observe stability also for a general choice of parameters. To validate the

unconditional stability property of the scheme also for general parameters, we perform additional numerical tests in section 5.

Theorem 2. *For $r = \rho = 0$ and $\mu = 1/2$ (Crank-Nicolson), the scheme (20) is unconditionally stable (von Neumann).*

Proof. We rewrite $u_{i,j}^n$ as

$$u_{i,j}^n = g^n e^{Iiz_1 + Ijz_2}, \tag{21}$$

where I is the imaginary unit, g^n is the amplitude at time level n, and $z_1 = 2\pi h/\lambda_1$ and $z_2 = 2\pi h/\lambda_2$ are phase angles with wavelengths λ_1 and λ_2, in the range $[-\pi, \pi]$, respectively. Then the scheme is stable if for all z_1 and z_2, the amplification factor $G = g^{n+1}/g^n$ satisfies the relation

$$|G|^2 - 1 \leq 0. \tag{22}$$

An expression for G can be found using (21) in (20).

Let us define new variables

$$c_1 = \cos\left(\frac{z_1}{2}\right), \quad c_2 = \cos\left(\frac{z_2}{2}\right), \quad s_1 = \sin\left(\frac{z_1}{2}\right), \quad s_2 = \sin\left(\frac{z_2}{2}\right),$$
$$W = -\frac{2s_2 s_1 \left(-\theta + vy\right)}{v}, \quad V = \frac{2vy}{\kappa},$$

which allow us to express G in terms of h, k, κ, V, W and trigonometric functions only. The new variable V has constant positive sign contrary to W.

In the new variables the stability criterion (22) of the scheme becomes

$$\frac{-8kh^2(n_4h^2 + n_2)}{d_6h^6 + d_4h^4 + d_2h^2 + d_0} \leq 0, \tag{23}$$

with

$$\begin{aligned}
n_4 &= -4V\kappa^3 f_3 s_1^4 h^2 W^2 - V^3\kappa^3 f_1 s_1^6 h^2, \quad n_2 = -4V^3\kappa^3 f_2 f_3 s_1^4,\\
d_6 &= 4\left(-2Wc_2 + Vs_1c_1\right)^2 \kappa^2 s_1^4,\\
d_4 &= \frac{1}{4}\kappa^4 s_1^4 \left(4VWs_1c_1c_2 - 4W^2 - s_1^2V^2\right)^2 k^2\\
&\quad - 4\kappa^3 V s_1^4 \left(s_1^2V^2 f_1 + 4f_3W^2\right) k + 16\kappa^2 V^2 {f_2}^2 s_1^4,\\
d_2 &= \left(s_1^2 f_5 V^2 - 36c_1 W s_1 c_2 V + 4f_4 W^2\right)\kappa^4 s_1^4 V^2 k^2 - 16V^3\kappa^3 f_2 f_1 s_1^4 k,\\
d_0 &= 4s_1^4 V^4 \kappa^4 f_1^2 k^2,
\end{aligned}$$

where f_1, f_2, f_3, f_4, and f_5 have constant sign and are defined by

$$\begin{aligned} f_1 &= 2c_1^2c_2^2 + c_1^2 + c_2^2 - 4 \leq 0, & f_2 &= c_1^2 + c_2^2 + 1 \geq 0, \\ f_3 &= 2c_1^2c_2^2 - c_1^2 - 1 \leq 0, & f_4 &= 4c_1^4c_2^2 - 2c_1^2 - c_2^2 + 8 \geq 0, \\ f_5 &= 4c_1^2{c_2}^4 - c_1^2 - 2c_2^2 + 8 \geq 0. \end{aligned}$$

We observe that we can restrict our analysis to the trigonometric functions s_1, s_2, c_1, and c_2 in the reduced range $[0, 1]$ (even exponents). It is straightforward to verify that n_4, n_2, d_6, d_4, and d_0 are positive. It remains to prove that $d_2 = d_{22}k^2 + d_{21}k$ is positive as well. Indeed, $d_{21} \geq 0$ and d_{22} is a polynomial of degree two in W having a positive leading order coefficient. The minimum value of d_{22} is given by

$$m = 2\kappa^4 s_1^6 V^4 f_1 f_6 / f_7$$

with

$$\begin{aligned} f_6 &= 4c_2^4c_1^4 - 2c_1^4c_2^2 - 2c_1^2c_2^4 + 6c_1^2c_2^2 + c_1^2 + c_2^2 - 8 \leq 0, \\ f_7 &= 4c_1^4c_2^2 - 2c_1^2 - c_2^2 + 8 \geq 0. \end{aligned}$$

Hence, m is positive and then d_2 is positive as well.

Therefore, the numerator in (23) is negative and the denominator in (23) is positive which completes the proof. ■

Finally using the Lax-Richtmyer equivalence theorem we can conclude convergence of the new scheme.

Theorem 3. *For $r = \rho = 0$, $\mu = 1/2$ (Crank-Nicolson), with well-posed initial value problem for the partial differential equation (10), the scheme (20) is convergent.*

Proof. The claim follows from the Lax-Richtmyer equivalence theorem, see, e.g., [15]. ■

5. Numerical results

5.1. Numerical convergence

In this section we perform a numerical study to compute the order of convergence of the scheme. Due to the compact discretization of (20) the

Parameter	Value
strike price	$K = 100$
time to maturity	$T = 0.5$
interest rate	$r = 0.05$
volatility of volatility	$v = 0.1$
mean reversion speed	$\kappa = 2$
long-run mean of σ	$\theta = 0.01$
correlation	$\rho = -0.5$

Table 1: Default parameters for numerical simulations.

resulting linear systems have a good sparsity pattern and can be solved very efficiently. We compute the l_2 norm error ε_2 and the maximum norm error ε_∞ of the numerical solution. We fix the parabolic mesh ratio k/h^2 to a constant value. Then, asymptotically, we expect these errors to converge as $\varepsilon = Ch^m$ for some m and C representing a constant. This implies $\ln(\varepsilon) = \ln(C) + m\ln(h)$. Hence, the double-logarithmic plot ε against h should be asymptotic to a straight line with slope m. This gives a method for experimentally determining the order of the scheme.

We refer to Figure 1 and Figure 2 for the results using the default parameters from Table 1. For the parameter μ, we use a Rannacher time-stepping choice [13], i.e., we start with four fully implicit quarter time steps ($\mu = 1$) and then continue with Crank-Nicolson ($\mu = 1/2$). For comparison we conducted additional experiments using a standard, second order scheme. We observe that the numerical convergence order agrees well with the theoretical order of the schemes for carefully smoothed initial condition. For non-smooth initial condition the numerical convergence order of the high order compact scheme is reduced to about two. The error in the maximum norm in this case, however, is still smaller by a factor $1.5 - 2$ than the error for the standard scheme for comparable numerical effort.

5.2. Validation of unconditional stability

In our numerical analysis in section 4.3, we have proven unconditional stability and convergence of our new scheme for $r = \rho = 0$. To validate the property of unconditional stability for general parameters, we perform additional numerical tests. We compute numerical solutions for varying values

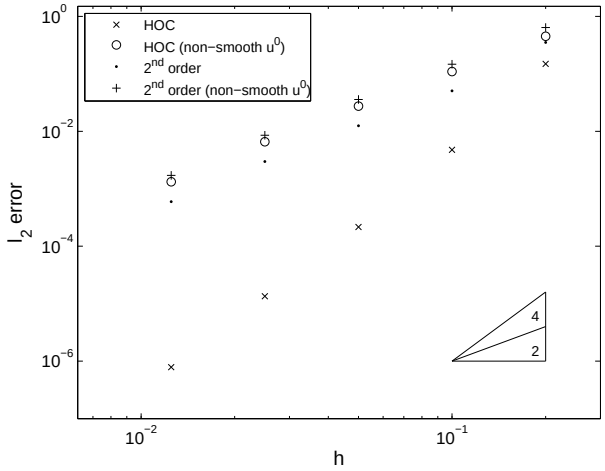

Figure 1: l_2-error vs. h.

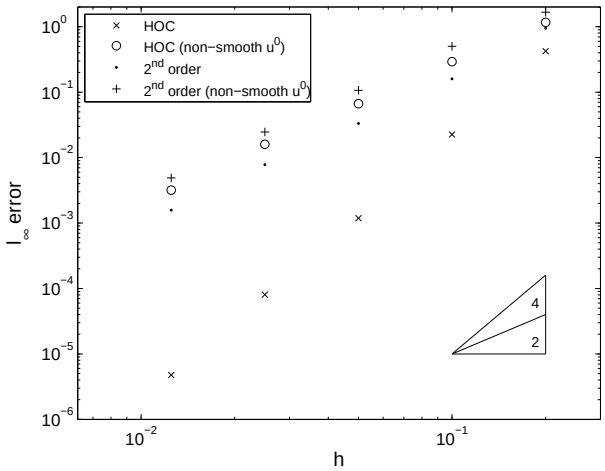

Figure 2: l_∞-error vs. h.

of the parabolic mesh ration k/h^2 and the mesh width h. Plotting the associated l_2-errors in the plane should allow us to detect stability restrictions depending on k/h^2 or oscillations that occur for high cell Reynolds number (large h). This approach for a numerical stability study was also used in [5]. We perform numerical experiments for $\rho = 0$ and $\rho = -0.5$. For the other parameters, we use again the default parameters from Table 1. The results

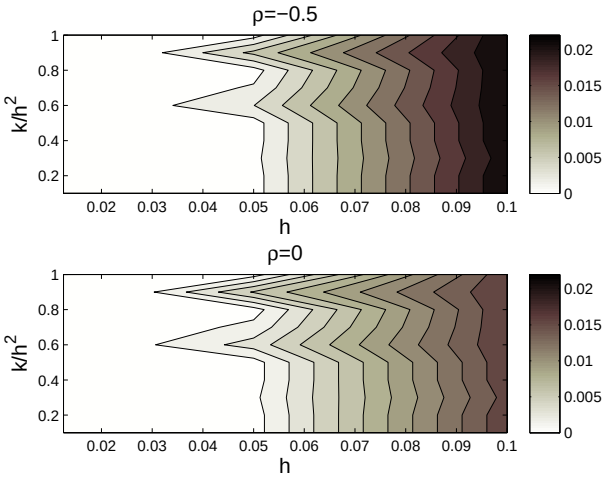

Figure 3: l_2-error in the k/h^2-h-plane for $\rho = -0.5$ (top) and $\rho = 0$ (bottom).

are shown in Figure 3. For both cases, $\rho = 0$ and $\rho = -0.5$, the errors show a similar behavior, being slightly larger for non-vanishing correlation. There is almost no dependence of the error on the parabolic mesh ratio k/h^2, which confirms the unconditional stability of the scheme. For larger values of h, which also result in a higher cell Reynolds number, the error grows gradually, and no oscillations in the numerical solutions occur. Based on this results we conjecture that the new scheme is unconditionally stable (and convergent) also for general choice of parameters.

5.3. Free boundary problem for the American option

In this section we present some numerical results for the American option case, where early exercise of the option is possible. This leads to an early exercise constraint, $V(S, \sigma, t) \geq V(S, \sigma, T)$, i.e., the option price is bounded from below by the payoff function. In the region of the time-spatial domain where this constraint is inactive, the option price solves (3). The boundary separating the two regions is not known a priori, thus one has to deal with a free boundary problem. Combining these relations leads to a complementarity problem of the form

$$Lu \geq 0, \quad u \geq u_0, \quad (Lu)(u - u_0) = 0, \qquad \text{for } x, y > 0,\ t > 0, \tag{24}$$

where L is the differential operator related to (9) and u_0 the payoff function (the early exercise constraint). The initial condition and the homogeneous

Neumann boundary conditions remain unchanged, while the Dirichlet boundaries have to be projected on the constraint.

For the numerical solution, we discretize (24) using the high-order compact scheme (20). We obtain a discrete matrix corresponding to (24). This can be solved by projected successive overrelaxation (PSOR). The method is widely used for solving the American option pricing problem. It amounts to solving the resulting linear system iteratively by a modified SOR method. In each SOR iteration step the new iterates are projected onto the constraint to guarantee that the early exercise constraint is fulfilled. The iteration stops once the residual falls below a prescribed stopping parameter. Hence, all iterates satisfy the constraint, and the final iterate is an approximate solution to (24).

Classical results state how the overrelaxation parameter in the SOR method can be chosen optimally depending on the eigenvalues of the iteration matrix. In our numerical experiments, we initially start with a suitable choice of the relaxation parameter and monitor the number of iterations needed to achieve the prescribed stopping criterion for the residual. As time evolves in our simulation we then adaptively increase or decrease the relaxation parameter according to these numbers.

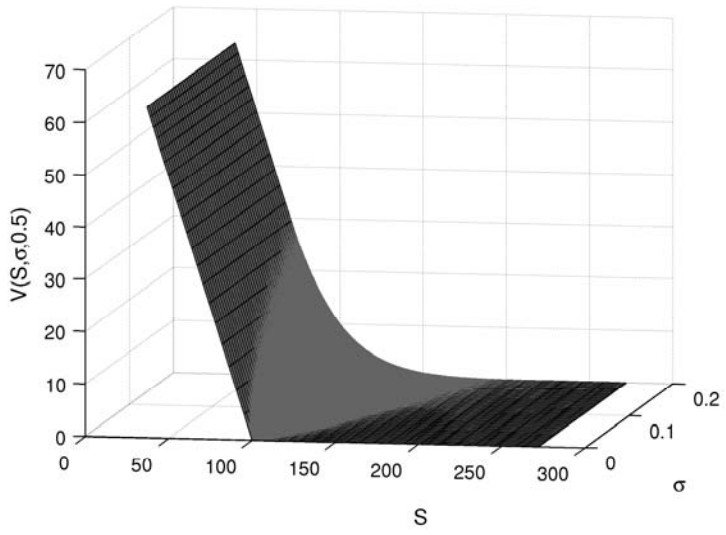

Figure 4: Numerical solution for the American option price and the early exercise constraint.

Figure 4 and Figure 5 show the numerical solutions for the American and

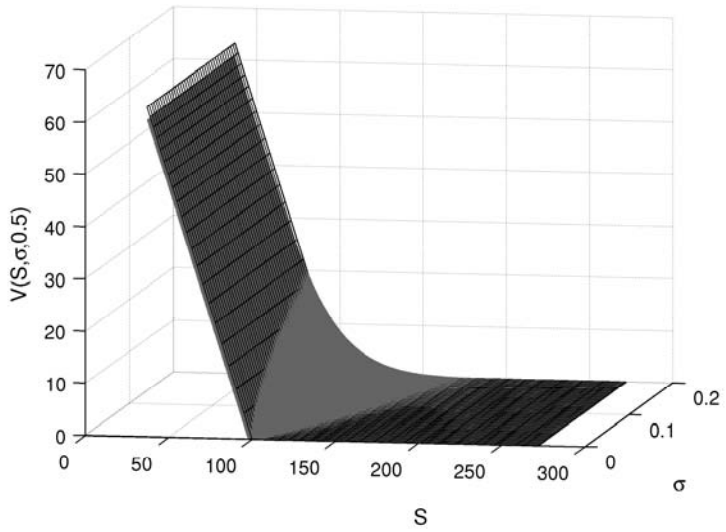

Figure 5: Numerical solution for the European option price and the initial condition.

the European option prices, respectively, using the default parameters from Table 1 together with the the constraint and initial condition, respectively. The PSOR iteration is stopped once the residual falls below $10^{-}6$. For the American option the option price surface joins smoothly onto the early exercise constraint which equals the payoff function while for the European option the surface intersects the payoff function.

Acknowledgement.
Bertram Düring acknowledges support from the Austrian Science Fund (FWF), grant P20214, and from the Austrian-Croatian Project HR 01/2010 of the Austrian Exchange Service (ÖAD).

References

[1] E. Benhamou, E. Gobet, and M. Miri. Time Dependent Heston Model, *SIAM J. Finan. Math.* **1**, 289-325, 2010.

[2] F. Black and M. Scholes. The pricing of options and corporate liabilities. *J. Polit. Econ.* **81**, 637-659, 1973.

[3] N. Clarke and K. Parrott. Multigrid for American option pricing with stochastic volatility. *Appl. Math. Finance* **6**(3), 177–195, 1999.

[4] B. Düring, M. Fournié and A. Jüngel. Convergence of a high-order compact finite difference scheme for a nonlinear Black-Scholes equation. *Math. Mod. Num. Anal.* **38**(2), 359–369, 2004.

[5] B. Düring, M. Fournié and A. Jüngel. High-order compact finite difference schemes for a nonlinear Black-Scholes equation. *Intern. J. Theor. Appl. Finance* **6**(7), 767–789, 2003.

[6] B. Düring. Asset pricing under information with stochastic volatility. *Rev. Deriv. Res.* **12**(2), 141–167, 2009.

[7] S.L. Heston. A closed-form solution for options with stochastic volatility with applications to bond and currency options. *Review of Financial Studies* **6**(2), 327–343, 1993.

[8] K.J. in't Hout and S. Foulon. ADI finite difference schemes for option pricing in the Heston model with correlation. *Int. J. Numer. Anal. Mod.* **7**, 303–320, 2010.

[9] S. Ikonen and J. Toivanen. Efficient numerical methods for pricing American options under stochastic volatility. *Numer. Methods Partial Differential Equations* **24**(1), 104–126, 2008.

[10] N. Hilber, A. Matache, and C. Schwab. Sparse wavelet methods for option pricing under stochastic volatility. *J. Comput. Financ.* **8**(4), 1–42, 2005.

[11] W. Liao and A.Q.M. Khaliq. High-order compact scheme for solving nonlinear Black-Scholes equation with transaction cost. *Int. J. Comput. Math.* **86**(6), 1009–1023, 2009.

[12] P. Kangro and R. Nicolaides. Far field boundary conditions for Black-Scholes equations. *SIAM J. Numer. Anal.* **38**, 1357–1368, 2000.

[13] R. Rannacher. Finite element solution of diffusion problems with irregular data. *Numer. Math.* **43**(2), 309–327, 1984.

[14] W.F. Spotz and C.F. Carey. Extension of high-order compact schemes to time-dependent problems. *Numer. Methods Partial Differential Equations* **17**(6), 657–672, 2001.

[15] J.C. Strikwerda. *Finite difference schemes and partial differential equations*. Second edition. Society for Industrial and Applied Mathematics (SIAM), Philadelphia, PA, 2004.

[16] D.Y. Tangman, A. Gopaul, and M. Bhuruth. Numerical pricing of options using high-order compact finite difference schemes. *J. Comp. Appl. Math.* **218**(2), 270–280, 2008.

[17] D. Tavella and C. Randall. *Pricing Financial Instruments: The Finite Difference Method*. John Wiley & Sons, 2000.

[18] W. Zhu and D.A. Kopriva. A spectral element approximation to price European options with one asset and stochastic volatility. *J. Sci. Comput.* **42**(3), 426–446, 2010.

[19] R. Zvan, P.A. Forsyth and K.R. Vetzal. Penalty methods for American options with stochastic volatility. *J. Comp. Appl. Math.* **91**(2), 199–218, 1998.